Nanoscale

PAPER

View Article Online
View Journal | View Issue



Cite this: *Nanoscale*, 2017, **9**, 14065

# Graphene oxide inhibits malaria parasite invasion and delays parasitic growth *in vitro*†

Kenry, ‡[a,b,c] Ying Bena Lim,‡[c,d] Mui Hoon Nai,[e] Jianshu Cao,[d,f] Kian Ping Loh [a,b,g] and Chwee Teck Lim *[a,b,c,d,e]

Received 14th August 2017,
Accepted 21st August 2017

DOI: 10.1039/c7nr06007f

rsc.li/nanoscale

The interactions between graphene oxide (GO) and various biological entities have been actively investigated in recent years, resulting in numerous potential bioapplications of these nanomaterials. Despite this, the biological interactions between GO and disease-causing protozoan parasites have not been well elucidated and remain relatively unexplored. Here, we investigate the *in vitro* interactions between GO nanosheets and a particular species of malaria parasites, *Plasmodium falciparum* (*P. falciparum*). We hypothesize that GO nanosheets may exhibit antimalarial characteristic *via* action mechanisms of physical obstruction of *P. falciparum* parasites as well as nutrient depletion. To ascertain this, we characterize the physical interactions between GO nanosheets, red blood cells (RBCs), and malarial parasites as well as the adsorption of several biomolecules necessary for parasitic survival and growth on GO nanosheets. Subsequent to establishing the origin of this antimalarial behavior of GO nanosheets, their efficiency in inhibiting parasite invasion is evaluated. We observe that GO nanosheets at various tested concentrations significantly inhibit the invasion of malaria parasites into RBCs. Furthermore, GO nanosheets delay parasite progression from the ring to the trophozoite stage. Overall, this study may further shed light on the graphene-parasite interactions and potentially facilitate the development of nanomaterial-based strategies for combating malaria.



## 1. Introduction

Graphene oxide (GO) is the oxygenated derivative of two-dimensional (2D) graphene.[1,2] Among the numerous 2D nanomaterials,[3–6] GO stands out due to its large surface area, unique bio-physico-chemical properties, and excellent *in vitro* and *in vivo* biocompatibility.[7] Therefore, it has been actively explored for a wide variety of biological and biomedical applications. These include biological sensing,[8,9] cellular imaging,[10,11] cell culture,[12–15] antibacterial[16,17] and antithrombotic[18] coatings, and cancer therapeutics.[19,20] Interestingly, these bioapplications hinge significantly on the molecular and cellular interactions between GO and various biological entities.

GO possesses a unique 2D structural feature which endows it a large surface area as a template for cargo loading.[21–23] It is a versatile nanomaterial whose basal plane and periphery are decorated with various oxygen-containing groups. In fact, their presence on the surface of GO enhances its dispersibility, solubility, and stability in aqueous media and facilitates its chemical functionalization.[1,2] At the same time, these hydrophilic functionalities and aromatic domains enable GO to interact specifically with a plethora of biomolecules, such as proteins, peptides, and amino acids.[24,25] In addition, they serve as pre-concentration platforms for biomolecules through electrostatic interaction or π–π stacking.[12,13,18] Intriguingly, GO is also known to display excellent biocompatibility and low toxicity.[3] It has been reported that GO possesses a lower cytotoxicity than carbon nanotubes.[26,27] Moreover, contrary to the hydrophobic pristine graphene, the hydrophilic GO can be taken up by cells with minimal toxic effects.[26,28] Importantly, GO has been demonstrated to induce negligible *in vivo* toxicity in animals at low and medium concentrations.[26,29] All these bio-physico-chemical features render the versatile GO highly advantageous for bioapplications, as compared to other carbon-based and 2D nanomaterials.[30,31] In particular, the exceptional biomolecule loading capability of GO coupled with its large surface area and excellent

[a]*NUS Graduate School for Integrative Sciences and Engineering, National University of Singapore, Singapore 117456*
[b]*Centre for Advanced 2D Materials and Graphene Research Centre, National University of Singapore, Singapore 117543*
[c]*Department of Biomedical Engineering, National University of Singapore, Singapore 117576. E-mail: ctlim@nus.edu.sg*
[d]*Singapore-MIT Alliance for Research and Technology (SMART) Centre, Infectious Diseases IRG, Singapore 138602*
[e]*Mechanobiology Institute, National University of Singapore, Singapore 117411*
[f]*Department of Chemistry, Massachusetts Institute of Technology, Cambridge, USA 02139*
[g]*Department of Chemistry, National University of Singapore, Singapore 117543*
†Electronic supplementary information (ESI) available. See DOI: 10.1039/c7nr06007f
‡These authors contributed equally to this work.

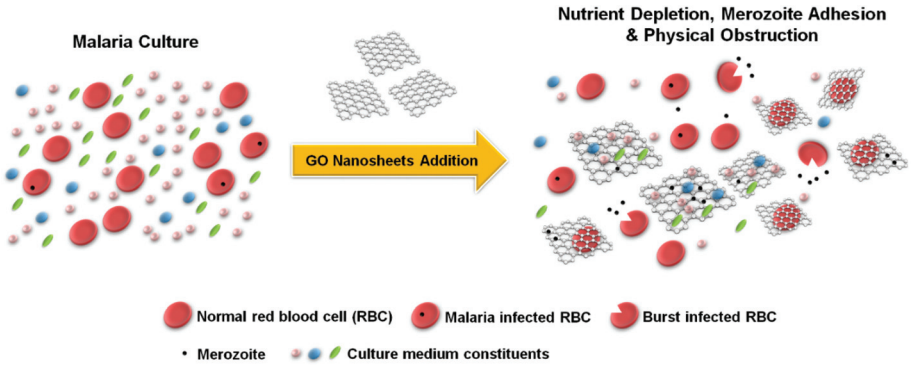


**Fig. 1** Schematic showing the hypothesized underlying mechanisms driving the potential antimalarial behavior of GO nanosheets (GOns). GOns are anticipated to display an antimalarial characteristic due to the superior loading capacity of GOns for biomolecules necessary for the growth and development of malaria parasites, leading to the depletion of nutrients for these parasites. Furthermore, GOns may play a key role as physical barriers in limiting the access of merozoites to healthy red blood cells (RBCs).

biocompatibility may potentially be exploited to obstruct the occurrence of specific biological events, such as cellular and/or parasitic growth, which form the basis of many physiological diseases.

Of all parasitic diseases, malaria remains one of the world's most prevalent and deadly infectious diseases and a global public health concern.[32,33] In 2013 alone, there were about 200 million clinical cases, with approximately 584 000 deaths worldwide.[34] This disease is caused by the protozoan parasites of the genus *Plasmodium*, which have a complex life cycle alternating between sexual and asexual reproduction in invertebrate mosquitoes and vertebrate hosts, respectively. In fact, the asexual malaria parasite infection in the peripheral blood circulation is the major cause behind the malarial disease pathology.[35] Among the *Plasmodium* parasite species responsible for human malaria infections, *Plasmodium falciparum* (*P. falciparum*) causes the highest rates of mortality and morbidity.[35,36] *P. falciparum* malaria parasites develop in two different hosts, *i.e.*, female Anopheles mosquito and human. In human, the malaria parasites taking the form of sporozoites enter the bloodstream and travel towards liver to start their multiplication. Over the course of several days, tens of thousands of merozoites will be produced and released into the bloodstream to invade circulating red blood cells (RBCs). Subsequently, throughout their 44–48 h asexual cycle within these RBCs, these malaria parasites mature and undergo different stages of development, *i.e.*, ring, trophozoite, and schizont, before the infected RBCs (iRBCs) burst and release more merozoites into the circulatory system. This part of the *Plasmodium* life cycle will repeat as merozoites invade even more healthy circulating RBCs.[37]

Here, using GO nanosheets (GOns) in aqueous suspension with distinct lateral size distributions and concentrations, we investigate the *in vitro* interactions between GOns and *P. falciparum* parasites. We hypothesize that due to their large specific surface area, GOns could play a key role in reducing malaria parasite invasion by physically trapping and obstructing the access of merozoites to RBCs. Furthermore, owing to their high loading capacity for biomolecules, these nanomaterials could reduce the availability of biomolecules necessary for parasite survival and invasion. Consequently, *via* these mechanisms, GOns are anticipated to exhibit antimalarial characteristic (Fig. 1).

## 2. Results and discussion

GOns in liquid suspension were first prepared using Hummer's method.[18] As numerous studies have reported the effect of size of graphene nanomaterials in influencing their interactions with various biological moieties,[38–40] we were also interested in characterizing this effect, specifically in affecting the possible antimalarial property of GOns. In yielding GOns with various lateral size distributions and mean lateral sizes, the as-prepared GOns (*i.e.*, GOns-0) were subsequently subjected to ultrasonication treatment for durations of 10, 60, and 120 min (*i.e.*, GOns-10, GOns-60, and GOns-120, respectively) (Fig. 2a), similar to that prepared in our previous work.[24] It is worth noting that GOns with distinct lateral size distributions were prepared using ultrasonication as the surface chemical properties of GOns would be minimally compromised.[16] Since GOns have irregular shapes, we defined the lateral size as the longest distance across a single nanosheet, similar to that described in reference.[41] Next, to acquire the statistical data on the lateral size distributions (Fig. S1a–d† and Fig. 2b) and mean lateral sizes (inset of Fig. 2b) of the different GOns samples, we examined approximately 400 nanosheets. In light of the experimental data, it was evident that the as-prepared GOns possessed distinct lateral size distributions and mean lateral sizes.

We next conjected that GOns with their large 2D surface area may serve as physical barriers that limit the access of merozoites to RBCs. This may be achieved through the direct physical attraction and trapping of merozoites onto the surface of GOns. To gain insights into the role of GOns in restricting merozoite accessibility, the physical interactions between

 

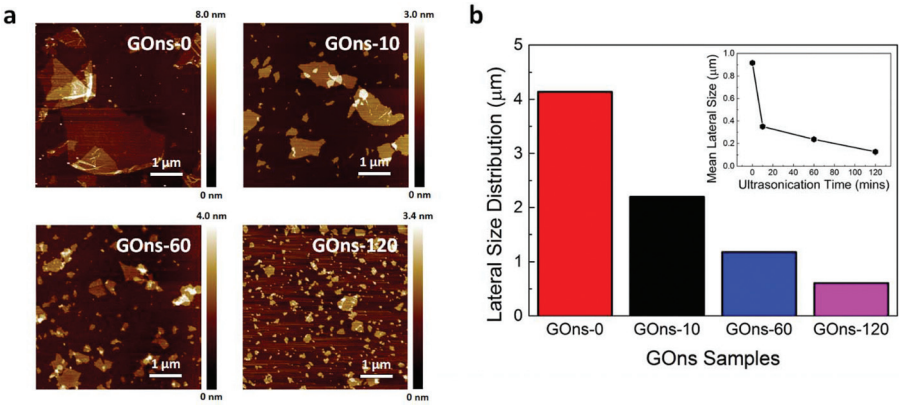


Fig. 2 Morphological characterization of GOns in liquid suspension. (a) Representative AFM topographical images of different GOns samples after undergoing ultrasonication treatment for different durations of 0, 10, 60, and 120 min (*i.e.*, GOns-0, GOns-10, GOns-60, and GOns-120, respectively). Scale bars represent 1 μm. (b) Lateral size distribution range of the different GOns samples. More than 400 nanosheets were assessed for each GOns sample. Inset illustrates the decreasing mean lateral sizes of GOns with ultrasonication time.

GOns, RBCs, and merozoites were probed using AFM. Firstly, magnetically enriched late stage iRBCs were incubated with RBCs at 2.5% hematocrit and 5% parasitemia as well as 6.25 μg $mL^{-1}$ GOns. A smear was then taken after a 12 h incubation when all iRBCs had burst and released their merozoites. The morphological shape and size distribution of the merozoites were next characterized. To ensure that merozoites were indeed the subject of characterization, the selected merozoites were those present around the ruptured iRBCs. We observed that these merozoites generally possessed ovoid bodies (Fig. S2a†) with an average length of 2.07 ± 0.86 μm (Fig. S2b†), similar to that reported in literature.[42] We subsequently investigated the physical interactions between GOns and RBCs by probing the healthy RBCs in the presence of GOns, but in the absence of merozoites. Interestingly, we noted that at the tested concentration, GOns exhibited a high degree of cellular hemocompatibility in that RBC maintained its structural integrity and did not experience hemolysis as the sharp edge of GOns did not damage nor penetrate the RBC membrane (Fig. 3a). Instead, GOns were able to conform smoothly to the shape of RBC (Fig. 3b). These observations revealed the excellent hemocompatibility of GOns in relation to their interactions with RBCs. After establishing the nanomaterial hemocompatibility, the GOns-RBC-merozoite interactions were examined to investigate if GOns could indeed act as physical barriers in mitigating the malarial parasite invasion. Here, again, we observed that large GOns fully covered and conformed to the shape of RBC. At the same time, multiple merozoites released from burst schizonts adhered onto the surface of GOns (Fig. 3c, as indicated by the white arrow, and Fig. 3d). The adhesion of these merozoites on the GOns surface physically limited their access to the healthy RBCs and greatly hindered the parasite invasion.

The interactions between GOns and malaria parasites were further evaluated through Giemsa and fluorescence staining (Fig. S3 and S4,† respectively). Here, merozoites were observed to adhere directly on the larger GOns (Fig. S3†). This phenomenon suggests a dependency and direct correlation between the parasite adhesion and the surface area of GOns. To ascertain this observation, GOns were next drop-casted on glass coverslips and incubated with iRBCs. After the rupture of iRBCs, the surface of the parasite-incubated GOns was stained with ethidium bromide (EtBr) to visualize the cellular contents of iRBCs, including merozoites, on the GOns surface under a confocal microscope (Fig. S4†). Fluorescence corresponding to the EtBr-stained merozoites, as depicted by the clusters of the small dots surrounding parasite nuclei, was highly expressed on all GOns. This further shows that GOns were able to physically attract the merozoites.

Numerous studies have demonstrated the superior loading capacity of graphene nanomaterials for various serums, proteins, and amino acids, which is beneficial for a plethora of cellular and physiological functions.[12,13,18] Depending on the nature of the interactions between proteins, cells, and graphene nanomaterials, the exceptional protein loading capacity of graphene nanomaterials may either enhance or hinder cellular development. The free amount of proteins in the system decreases as they get adsorbed on the nanomaterial surface. Consequently, cells which do not interact with the protein-loaded graphene nanomaterials may likely be deprived from the essential nutrients and growth factors, impeding cellular growth and proliferation. On this basis, we hypothesized that the hydrophilic GOns might possess a high loading capacity for various proteins, notably albumax II, in the malaria culture medium (MCM). This would lead to nutrient depletion for parasitic growth, resulting in the potential antimalarial behavior of GOns. To verify this, we evaluated the loading of individual MCM constituents on various GOns samples. Typically, MCM consists of tissue culture medium RPMI supplemented with serum protein albumax II, the purine source hypoxanthine, and the antibiotic gentamicin.[43] Albumax II is serum albumin known to be lipid-carrying in blood and is essential for the optimal growth of malaria parasites.[44] Hypoxanthine is a purine derivative necessary for

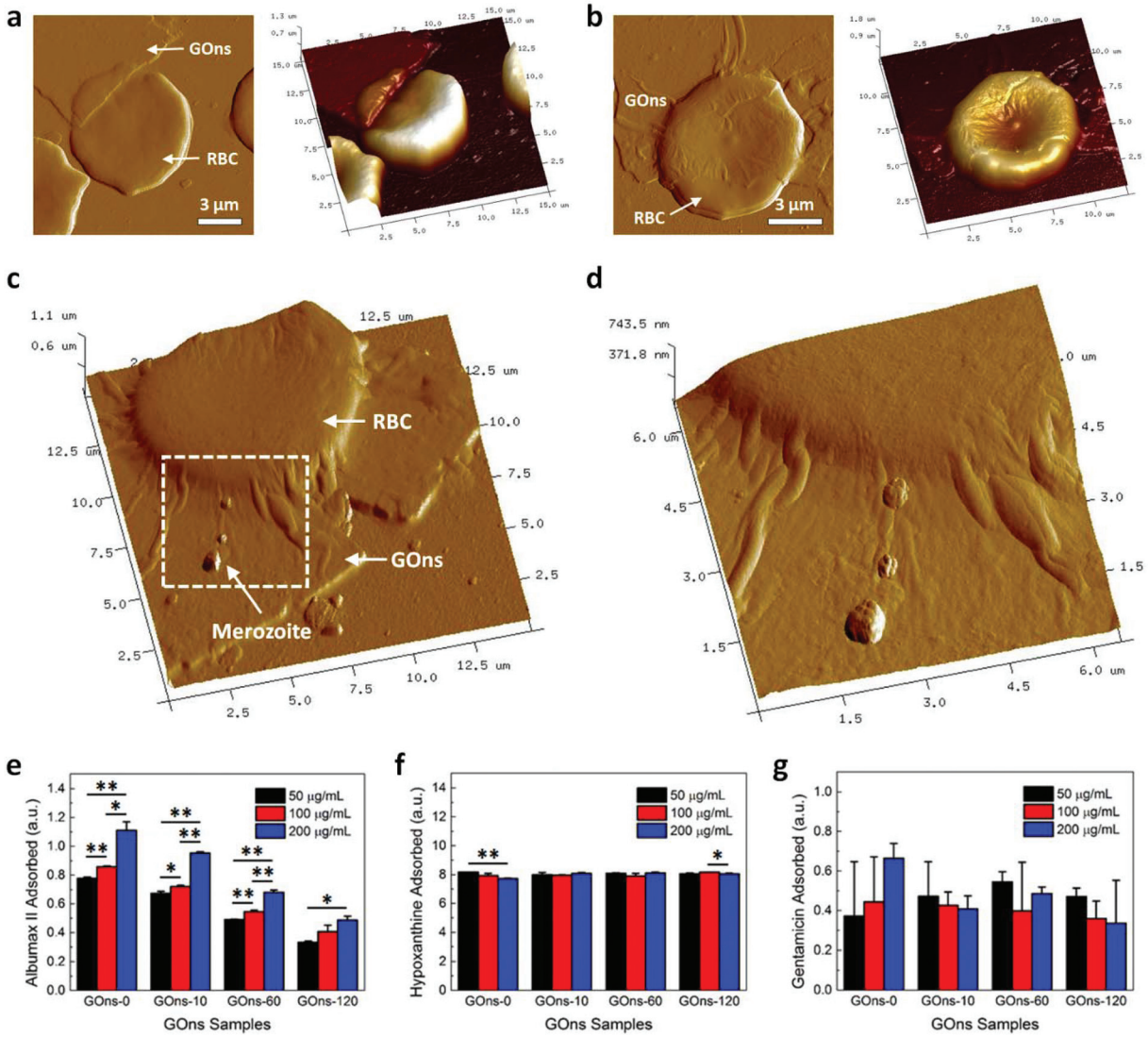


**Fig. 3** Mechanisms underlying the potential antimalarial characteristic of GOns. (a–d) Physical interactions between GOns, RBCs, and malaria parasites: (a–b) representative AFM amplitude (left) and topographical (right) images of the physical interactions between GOns and RBCs showing the (a) cellular hemocompatibility and (b) conformability of GOns on RBCs. All scale bars represent 3 μm. (c) Representative AFM topographical image showing the physical interaction between GOns, RBC, and merozoites. (d) Enlarged view of the region indicated by a white dotted box in (c), illustrating the adherence of merozoites on GOns and the inaccessibility of these merozoites to RBC. (e–g) Loading capacities of individual MCM constituents on GOns: (e) Albumax II, (f) hypoxanthine, and (g) gentamicin. The * and ** indicate statistically significant differences for $p < 0.05$ and 0.01, respectively, based on the two-tailed student's *t*-test.

the synthesis of nucleic acids and energy metabolism of the parasites as well as for the significant enhancement of their propagation.[45] Gentamicin, meanwhile, serves as a water-soluble aminoglycoside bactericidal antibiotic in the complete culture medium.[46] The relationship between the lateral size of GOns, their loading capacity for individual MCM constituents, and the potential antimalarial property of GOns were subsequently investigated.

We first measured the free absorbance of albumax II (Fig. S5a†), hypoxanthine (Fig. S5b†), and gentamicin (Fig. S5c†) prepared at various concentrations at the corresponding characteristic wavelengths of 280 nm, 260 nm, and 192 nm, respectively. A linear relationship was observed between the free absorbance of these MCM constituents and their concentrations (insets of Fig. S5a–c†). Next, we assessed the absorbance of albumax II, hypoxanthine, and gentamicin after incubating with GOns to evaluate the adsorption capacity of the individual MCM components on various GOns samples. The MCM constituents were fixed at a particular concentration and those of GOns were varied. After 48 h incubation, we observed a GOns concentration- and size-dependent adsorption of albumax II (Fig. 3e). As the concentration of GOns was increased from 50 μg $mL^{-1}$ to 200 μg $mL^{-1}$, the amount of adsorbed albumax II increased correspondingly. Interestingly, we noted that at particular GO concentrations, GOns-0 with the largest lateral size distribution and mean lateral size

 

consistently exhibited the highest loading capacity for albumax II. The lowest adsorption was found with GOns-120 which has the smallest average size and size distribution. This observation implies a probable GOns size-dependent loading of albumax II on GOns. Also, more importantly, it highlights that the adsorption of albumax II was significantly dependent on the concentration of GOns. The GOns-albumax II association might be primarily driven by the hydrophobic interactions between GOns and the hydrophobic regions of albumax II, coupled with electrostatic interactions.[47–49] Nonetheless, the GOns concentration-dependent loading capacity of biomolecules on GOns was not observed for both hypoxanthine and gentamicin (Fig. 3f and g), possibly due to their lower binding association and affinity to GOns. Several investigations have, in fact, revealed that the essential serum albumin serves as a critical source of nutrients for intraerythrocytic growth and cell cycle development of *P. falciparum* malaria parasites. It has also been emphasized that the intraerythrocytic parasites are able to uptake, breakdown, and degrade serum albumin, leading to a time-dependent proteolysis within the parasites.[50] In addition, recent evidences have suggested that *P. falciparum* parasites respond negatively to starvations of proteins and amino acids, indicating their dependence on exogenous nutrients.[51,52] Consequently, due to their exceptional loading capacity for MCM constituents, especially for serum albumin albumax II, GOns are anticipated to possess antimalarial behavior. It is important to highlight that while certain blood proteins might also get adsorbed on GOns surface,[15,18,24,25] the proper functioning of RBCs should not be affected as their primary function in facilitating oxygen transportation would typically be affected only in the event of hemolysis.

Following the elucidation of the possible mechanisms underlying the anticipated antimalarial behavior of GOns, we sought to evaluate their efficiency in inhibiting the invasion of *P. falciparum* parasites. Enriched infected erythrocytes of the laboratory adapted 3D7 strain were mixed with healthy blood and incubated in MCM in the presence of various GOns samples for 48 h. Smears for individual samples were made and stained with Giemsa before determining the parasitemia *via* counting approximately 1000 cells (Fig. 4a). The complete MCM and MCM diluted with different percentages of RPMI served as negative and positive controls, respectively. In light of the collated data, we observed that GOns exhibited a concentration-dependent antimalarial behavior by significantly inhibiting the parasite invasion of RBCs (Fig. 4b). Specifically, the invasion efficiency of the malaria parasites decreased progressively along with an increasing concentration of GOns from 6.25 μg $mL^{-1}$ to 50 μg $mL^{-1}$. Invasion efficiency is determined by normalizing the parasitemia to that of control, which is taken to be 100%. Intriguingly, even at a low concentration of 6.25 μg $mL^{-1}$, the parasite invasion efficiency due to GOns was significantly lower than that of negative control and similar to that of 25% MCM. Further increase in the concentration of GOns to 50 μg $mL^{-1}$ resulted in a greater decrease in the parasite invasion efficiency as compared to that of positive controls. It is interesting to note that all GOns exhibited similar parasite inhibition efficiency despite variations in albumax II adsorption on different GOns samples. As pointed out earlier, the antimalarial property of GOns might not be solely dependent on the depletion of nutrients through albumax II adsorption. GOns might also physically restrict the access of merozoites to RBCs. Therefore, this antimalarial characteristic of GOns was likely to be dependent on the intricate interplay between serum albumin adsorption and physical blocking of RBCs from merozoites.

Next, the effects of GOns on parasite maturation were examined. Interestingly, a recent study has demonstrated that *P. falciparum* parasites are capable of delaying their maturation in response to amino acid depletion in order to survive prolonged starvation.[52] As such, we postulated the occurrence of a similar phenomenon if GOns were able to absorb sufficient amount of albumax II to starve the parasites. To verify this, we monitored the development of tightly synchronized parasites (3 h) at three specific transitional stages, *i.e.*, from rings to trophozoites, from trophozoites to schizonts, and from schizonts to rings of the next life cycle, in the absence and presence of GOns. Here, GOns with two different effective concentrations of 6.25 μg $mL^{-1}$ ($GOns_{Low}$) and 50 μg $mL^{-1}$ ($GOns_{High}$) were added to the parasite cultures at 0 h, 24 h, and 36 h post-infection (HPI) when the synchronized parasite cultures were in the ring, trophozoite, and schizont stage, respectively (Fig. 4c). As before, MCM and MCM diluted with RPMI were correspondingly used as negative and positive controls. Smears of the cultures were taken at multiple HPIs, *i.e.*, 24 ± 3 h, 36 ± 3 h, and 46 ± 3 h, to ensure that observations were not due to asynchrony of the cells. We observed that the progression of malaria parasites was delayed from rings to trophozoites in the presence of $GOns_{High}$ and solely in RPMI (Fig. 4d). In fact, these parasites remained largely in the ring stage even when those cultured solely in MCM and in the presence of $GOns_{Low}$ had progressed to trophozoites at 21 h, 24 h, and 27 h. As compared to $GOns_{Low}$, $GOns_{High}$ exhibited a more pronounced effect in delaying the development of parasites from rings to trophozoites, plausibly due to the higher amount of albumax II adsorbed from the medium. Nevertheless, it is likely that the transition delay observed from rings to trophozoites was temporary considering that most of the infected cells were in the trophozoite stage when parasitemia was assessed after 48 h of culturing late stage infected cells in the previous section. Additionally, this stage transition delay was only evident when GOns were introduced while the parasites were still in the ring stage. The addition of GOns at 24 h and 36 h (*i.e.*, when the parasites were in the trophozoite and schizont stage, respectively) did not hamper the maturation of these parasites to schizonts and rings, respectively (Fig. S6†).

To gain further insights into the GOns-induced delayed maturation of parasites from rings to trophozoites, we characterized the presentation of knobs on the surface of iRBCs in the absence and presence of GOns. One of the key features corresponding to the asexual growth of malaria parasites is the

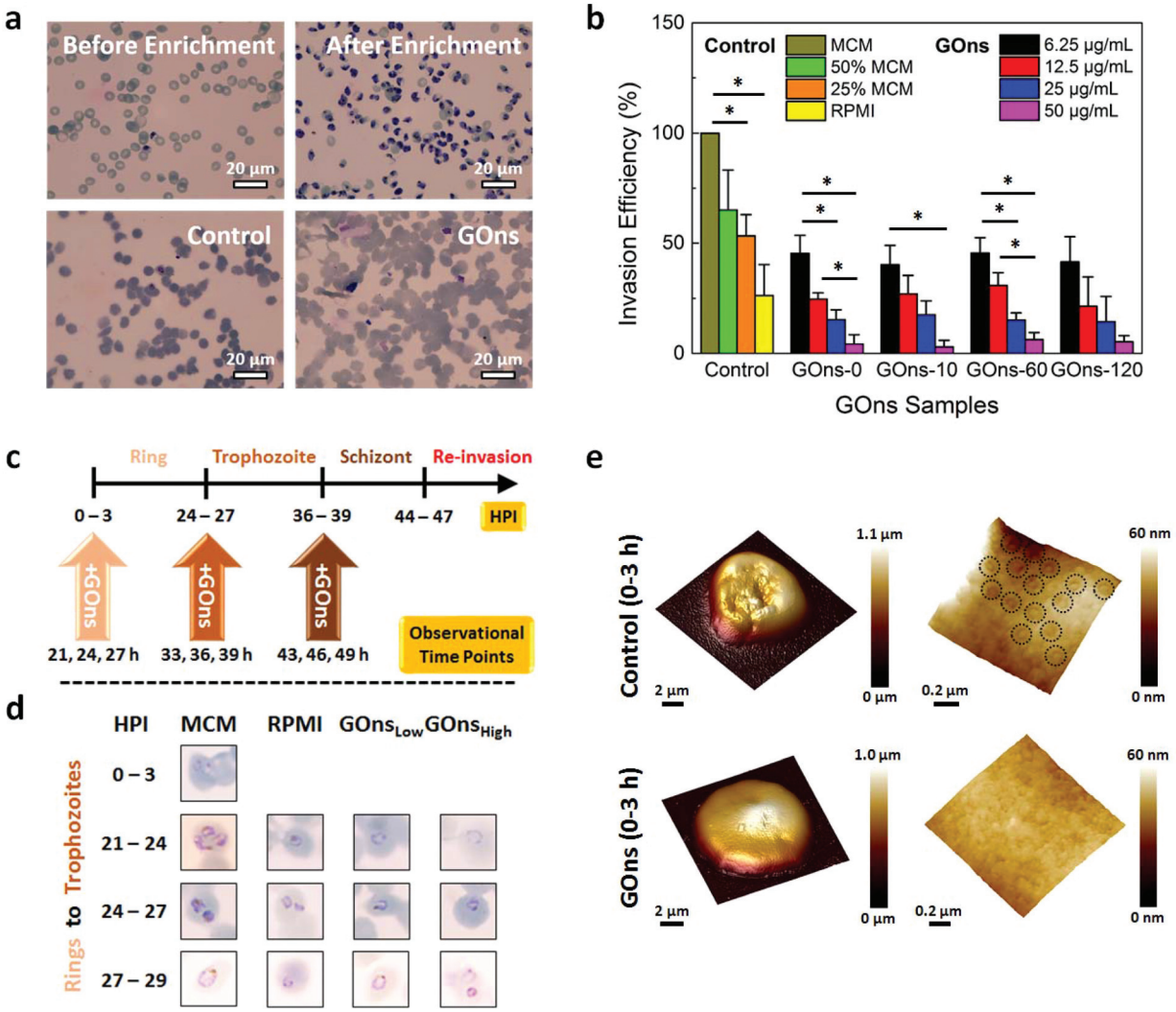


**Fig. 4** Inhibition of the invasion of *P. falciparum* malaria parasites by GOns, effects induced by GOns on the development of *P. falciparum* malaria parasites, and presentation of knobs on the surface of iRBCs in the absence and presence of GOns. (a) Representative Giemsa-stained images showing the amount of late stage *P. falciparum* parasites before and after MACS magnetic enrichment as well as in the presence of control and GOns. Scale bars represent 20 μm. (b) Invasion efficiency of the malaria parasites in the presence of GOns comparing the performance of specific GOns samples (*i.e.*, GOns-0, GOns-10, GOns-60, and GOns-120) with different concentrations against controls. The * indicates statistically significant differences for $p < 0.05$ based on the two-tailed student's *t*-test. (c) GOns with low and high concentrations (*i.e.*, 6.25 μg $mL^{-1}$ and 50 μg $mL^{-1}$, respectively) were added at 0 h, 24 h, and 36 h post-infection (HPI), when the malaria parasites were at the ring, trophozoite and schizont stage, respectively. (d) Giemsa-stained images showing iRBCs in the presence of MCM, RPMI, $GOns_{Low}$ (*i.e.*, 6.25 μg $mL^{-1}$), and $GOns_{High}$ (*i.e.*, 50 μg $mL^{-1}$), taken at time points during the maturation of the parasites from rings to trophozoites. (e) Morphology of iRBCs in the absence and presence of GOns introduced into the malaria culture at 0–3 h. Surface morphology of the cultured samples was characterized at 39–42 h (left) to evaluate the presentation of knobs, as indicated by the black dotted circles in the enlarged view of the iRBC surface for control but not GOns (right).

presentation of nanoscale protrusions or knobs on the iRBC surface due to the transport of knob-associated proteins from the parasites to erythrocytes.[53,54] In fact, the quantity and size of knobs found on the iRBC surface have been demonstrated to be directly correlated to the stage of infection[55] as knobs are typically manifested on iRBCs when the parasites have matured to trophozoite and beyond. As such, the denser and more concentrated the knobs exhibited on the iRBC surface, the more advanced the stage of parasite development.[55] GOns were introduced into the malaria culture at 0–3 h and 24–27 h. The surface morphology of the cultured iRBC samples was then characterized at 39–42 h. For control cultures, densely distributed surface knobs were observed, as expected (Fig. 4e and Fig. S7†). However, when GOns were introduced at 0 h, the knobs on the surface of iRBCs could hardly be observed even at 39–42 h (Fig. 4e). These knob characterization results corroborated with our previous observation in which GOns delayed the maturation of malaria parasites from rings to trophozoites. Cultures with GOns added at 24–27 h also showed distinct knobs on the iRBC surface at 39–42 h (Fig. S7†). This indicates that GOns did not affect the trophozoite-stage iRBCs from expressing knobs on their surface.

 

# 3. Conclusions

In summary, we investigated the *in vitro* interactions between GOns and malaria parasites. The mechanisms leading to the possible antimalarial behavior of GOns, *i.e.*, physical obstruction, merozoite adhesion, and nutrient depletion were first examined. The adhesion of merozoites to the physical barrier GOns could hinder the invasion of RBCs. Additionally, the high loading capacity of GOns for the constituents of MCM likely caused the depletion of nutrients necessary for the growth and invasion of *P. falciparum* parasites. We further demonstrated the reduction in parasite invasion efficiency by GOns. Experimental results showed that GOns displayed a concentration-dependent antimalarial behavior by significantly inhibiting the invasion of malaria parasites into RBCs. We also observed that GOns induced a stage transition delay which interrupted the maturation of malaria parasites from rings to trophozoites. Overall, we anticipate that this study will be beneficial for the further exploration of nanomaterials-based approaches in malaria research.

# 4. Experimental section

### GO nanosheet preparation and characterization

GOns in aqueous solution were first prepared based on Hummer's method. They were then subjected to ultrasonication treatment (SONICS, VCX-130) at 40% amplitude for 15 s ON and 5 s OFF cycles, for different durations of 10, 60, and 120 min to yield GOns with various lateral size distributions and mean lateral sizes. Atomic force microscope (AFM) (Bruker, Billerica, MA) operating under the tapping mode was used to characterize the surface morphological features of the GOns samples in liquid suspension dropped on freshly cleaved mica. Using ImageJ software (NIH, US), the lateral size distributions of GOns in aqueous solution were estimated from the obtained AFM images. Roughly 400 GOns were assessed to calculate their lateral size distributions and mean lateral sizes.

### Biomolecule loading capacity assay

Individual constituents of MCM – Albumax II (Gibco Invitrogen), hypoxanthine (Sigma Aldrich), and gentamicin reagent (Life Technologies) – were prepared in 1× PBS at a concentration of 2 mg $mL^{-1}$. GOns in liquid suspension were prepared at different concentrations of 50, 100, and 200 μg $mL^{-1}$. The MCM constituents (30 μL) were then mixed with GOns (30 μL) and the resultant mixtures were incubated at 37 °C for 48 h. After the incubation, the mixtures were centrifuged at 13 000*g* for 10 min and the supernatants were collected for spectrophotometric measurements. Using the UV-Vis spectrophotometer (NanoDrop 2000, Thermo Scientific), the adsorption isotherm of each MCM constituent was obtained. Three independent readings under room temperature were acquired for each absorption spectrum. The adsorption of each MCM constituent on GOns was subsequently determined from the difference in protein adsorption pre- and post-addition of GOns.

### Sample preparation and AFM imaging

For imaging of iRBCs, the smears of suspension cultures (*i.e.*, 2.5% hematocrit, 1% parasitemia with 10% of 62.5 μg $mL^{-1}$ GOns of all sizes) were made and dried on a hotplate at 40 °C for 30 min. For imaging of the physical interactions between GOns, RBCs, and merozoites, magnetically enriched late stage iRBCs were incubated with RBCs at 2.5% hematocrit and 5% parasitemia as well as 10% of 62.5 μg $mL^{-1}$ GOns of various sizes in the culture. A smear was made 12 h later when all iRBCs had burst and the merozoites had been released into the culture. Slides were stored in a dehumidified chamber before imaging. All samples were imaged with a Bruker Dimension FastScan AFM system operating in PeakForce Tapping mode. AFM images were acquired with a Bruker FastScan-B cantilever (spring constant 4 N $m^{-1}$) at a maximum scan rate of 2 Hz and 512 × 512 data points per image. Raw AFM data were processed using Bruker Nanoscope Analysis 1.50 software.

### Merozoite adhesion assay, fluorescence staining, and imaging

100 μL liquid solutions of 50 μg $mL^{-1}$ GOns with different lateral size distributions and mean lateral sizes were drop-casted on 18 mm glass coverslips and heated at 120 °C to produce solid GOns substrates. Approximately 200 μL of enriched infected erythrocyte suspension (0.5% by volume in MCM) was then seeded on each solid GOns substrate. After the iRBCs burst, these solid GOns substrates were washed gently in 1× PBS to remove any cellular components that did not stick onto the substrates. Eventually, after a five minute incubation with 10 mg $mL^{-1}$ ethidium bromide, Zeiss confocal microscope was used to obtain the fluorescent images of the cellular contents adhered on the solid GOns substrates.

### Malaria invasion assay

Synchronized and enriched infected erythrocytes were first added to healthy blood (1% parasitemia) to form a mixture. In each well of the 96-well plate, 175 μL of malaria culture medium (MCM) was added together with 5 μL of infected blood mixture and 20 μL of the GOns samples (*i.e.*, GOns-0, GOns-10, GOns-60, and GOns-120 at different concentrations of 62.5, 125, 250, and 500 μg $mL^{-1}$). As a negative control, 5 μL of infected blood mixture was added to 175 μL of MCM and 20 μL of MilliQ water. Positive controls replaced MCM in the negative control with RPMI (*i.e.*, 50%, 75%, and 100% RPMI). The filled 96-well plate was then incubated for 48 h. A smear was made for each well and stained with Giemsa after fixing with methanol. Each smear was observed under an optical microscope using a 100× oil objective. At least 1000 cells were counted for each smear to obtain the parasitemia. Three independent experiments were performed and the obtained results were averaged.

### Parasite stage development assay

Laboratory strain of *Plasmodium falciparum*, 3D7, was tightly synchronized with sorbitol prior to the experiment within a

3 h window. Three sets of cultures, consisting of 12 wells each, were seeded in a 96-well plate at 0–3 h post-infection with 0.5% parasitemia and 2.5% hematocrit. At 0 h, GOns in liquid suspension were introduced to the first set of cultures, *i.e.*, four cultures with 10% of 62.5 μg $mL^{-1}$ of GOns (*i.e.*, GOns-0, GOns-10, GOns-60, and GOns-120) and four cultures with 10% of 500 μg $mL^{-1}$ of GOns. For comparison, MCM in the remaining four cultures was replaced with varying amounts of RPMI such that the cultures contained 100% MCM, 50% MCM, 25% MCM, and 0% MCM. Smears were fixed and stained with Giemsa at 21, 24, and 27 h. Similar steps were performed on the second and third sets at 24 h (observed at different time points of 33, 36, and 39 h) and 36 h (observed at different time points of 43, 46, and 49 h), respectively.

## Conflicts of interest

There are no conflicts to declare.

## Acknowledgements

Kenry and Y. B. Lim contributed equally to this work. Kenry would like to acknowledge NUS Graduate School for Integrative Sciences and Engineering Scholarship. Y. B. Lim would like to acknowledge SMA Graduate Fellowship at SMART. K. P. Loh wishes to acknowledge funding support from NRF-investigatorship award NRF-NRF12015-01 "Graphene oxide a new class of catalytic, ionic and molecular sieving materials." This research was supported by the National Research Foundation, Prime Minister's Office, Singapore under its medium-sized centre programme, Centre for Advanced 2D Materials and its Research Centre of Excellence, Mechanobiology Institute, as well as the MechanoBioEngineering Laboratory of the Department of Biomedical Engineering of the National University of Singapore.

## References

1 D. R. Dreyer, S. Park, C. W. Bielawski and R. S. Ruoff, *Chem. Soc. Rev.*, 2010, **39**, 228–240.
2 S. Eigler and A. Hirsch, *Angew. Chem., Int. Ed.*, 2014, **53**, 7720–7738.
3 Kenry and C. T. Lim, *ChemNanoMat*, 2017, **3**, 5–16.
4 Kenry, A. Geldert, X. Zhang, H. Zhang and C. T. Lim, *ACS Sens.*, 2016, **1**, 1315–1321.
5 A. Geldert, Kenry, X. Zhang, H. Zhang and C. T. Lim, *Analyst*, 2017, **142**, 2570–2577.
6 Kenry, A. Geldert, Z. Lai, Y. Huang, P. Yu, C. Tan, Z. Liu, H. Zhang and C. T. Lim, *Small*, 2017, **13**, 1601925.
7 S. A. Sydlik, S. Jhunjhunwala, M. J. Webber, D. G. Anderson and R. Langer, *ACS Nano*, 2015, **9**, 3866–3874.
8 Y. Liu, D. Yu, C. Zeng, Z. Miao and L. Dai, *Langmuir*, 2010, **26**, 6158–6160.
9 A. M. H. Ng, Kenry, C. Teck Lim, H. Y. Low and K. P. Loh, *Biosens. Bioelectron.*, 2015, **65**, 265–273.
10 Q. Liu, L. Wei, J. Wang, F. Peng, D. Luo, R. Cui, Y. Niu, X. Qin, Y. Liu, H. Sun, J. Yang and Y. Li, *Nanoscale*, 2012, **4**, 7084–7089.
11 J. Li, W. Zhang, T.-F. Chung, M. N. Slipchenko, Y. P. Chen, J.-X. Cheng and C. Yang, *Sci. Rep.*, 2015, **5**, 12394.
12 W. C. Lee, C. H. Y. X. Lim, H. Shi, L. A. L. Tang, Y. Wang, C. T. Lim and K. P. Loh, *ACS Nano*, 2011, **5**, 7334–7341.
13 W. C. Lee, C. H. Lim, Kenry, C. Su, K. P. Loh and C. T. Lim, *Small*, 2015, **11**, 963–969.
14 T.-H. Kim, S. Shah, L. Yang, P. T. Yin, M. K. Hossain, B. Conley, J.-W. Choi and K.-B. Lee, *ACS Nano*, 2015, **9**, 3780–3790.
15 Kenry, P. K. Chaudhuri, K. P. Loh and C. T. Lim, *ACS Nano*, 2016, **10**, 3424–3434.
16 S. Liu, M. Hu, T. H. Zeng, R. Wu, R. Jiang, J. Wei, L. Wang, J. Kong and Y. Chen, *Langmuir*, 2012, **28**, 12364–12372.
17 J. Zhao, B. Deng, M. Lv, J. Li, Y. Zhang, H. Jiang, C. Peng, J. Li, J. Shi, Q. Huang and C. Fan, *Adv. Healthcare Mater.*, 2013, **2**, 1259–1266.
18 Kenry, K. P. Loh and C. T. Lim, *Small*, 2015, **11**, 5105–5117.
19 Z. Liu, J. T. Robinson, X. Sun and H. Dai, *J. Am. Chem. Soc.*, 2008, **130**, 10876–10877.
20 X. Zhao, L. Yang, X. Li, X. Jia, L. Liu, J. Zeng, J. Guo and P. Liu, *Bioconjugate Chem.*, 2015, **26**, 128–136.
21 H. Yue, W. Wei, Z. Yue, B. Wang, N. Luo, Y. Gao, D. Ma, G. Ma and Z. Su, *Biomaterials*, 2012, **33**, 4013–4021.
22 C. Chung, Y.-K. Kim, D. Shin, S.-R. Ryoo, B. H. Hong and D.-H. Min, *Acc. Chem. Res.*, 2013, **46**, 2211–2224.
23 V. Georgakilas, J. N. Tiwari, K. C. Kemp, J. A. Perman, A. B. Bourlinos, K. S. Kim and R. Zboril, *Chem. Rev.*, 2016, **116**, 5464–5519.
24 Kenry, K. P. Loh and C. T. Lim, *Nanoscale*, 2016, **8**, 9425–9441.
25 Kenry, K. P. Loh and C. T. Lim, *RSC Adv.*, 2016, **6**, 46558–46566.
26 C. Fisher, A. E. Rider, Z. Jun Han, S. Kumar, I. Levchenko and K. Ostrikov, *J. Nanomater.*, 2012, **2012**, 315185.
27 Y. Zhang, S. F. Ali, E. Dervishi, Y. Xu, Z. Li, D. Casciano and A. S. Biris, *ACS Nano*, 2010, **4**, 3181–3186.
28 A. Sasidharan, L. S. Panchakarla, P. Chandran, D. Menon, S. Nair, C. N. R. Rao and M. Koyakutty, *Nanoscale*, 2011, **3**, 2461–2464.
29 K. Wang, J. Ruan, H. Song, J. Zhang, Y. Wo, S. Guo and D. Cui, *Nanoscale Res. Lett.*, 2011, **6**, 8.
30 M. Xu, J. Zhu, F. Wang, Y. Xiong, Y. Wu, Q. Wang, J. Weng, Z. Zhang, W. Chen and S. Liu, *ACS Nano*, 2016, **10**, 3267–3281.
31 R. Kurapati, K. Kostarelos, M. Prato and A. Bianco, *Adv. Mater.*, 2016, **28**, 6052–6074.
32 P. D. Crompton, S. K. Pierce and L. H. Miller, *J. Clin. Invest.*, 2010, **120**, 4168–4178.
33 P. A. Buffet, I. Safeukui, G. Deplaine, V. Brousse, V. Prendki, M. Thellier, G. D. Turner and O. Mercereau-Puijalon, *Blood*, 2011, **117**, 381–392.

 

34 B. Baragana, I. Hallyburton, M. C. S. Lee, N. R. Norcross, R. Grimaldi, T. D. Otto, W. R. Proto, A. M. Blagborough, S. Meister, G. Wirjanata, A. Ruecker, L. M. Upton, T. S. Abraham, M. J. Almeida, A. Pradhan, A. Porzelle, M. S. Martinez, J. M. Bolscher, A. Woodland, S. Norval, F. Zuccotto, J. Thomas, F. Simeons, L. Stojanovski, M. Osuna-Cabello, P. M. Brock, T. S. Churcher, K. A. Sala, S. E. Zakutansky, M. B. Jimenez-Diaz, L. M. Sanz, J. Riley, R. Basak, M. Campbell, V. M. Avery, R. W. Sauerwein, K. J. Dechering, R. Noviyanti, B. Campo, J. A. Frearson, I. Angulo-Barturen, S. Ferrer-Bazaga, F. J. Gamo, P. G. Wyatt, D. Leroy, P. Siegl, M. J. Delves, D. E. Kyle, S. Wittlin, J. Marfurt, R. N. Price, R. E. Sinden, E. A. Winzeler, S. A. Charman, L. Bebrevska, D. W. Gray, S. Campbell, A. H. Fairlamb, P. A. Willis, J. C. Rayner, D. A. Fidock, K. D. Read and I. H. Gilbert, *Nature*, 2015, **522**, 315–320.

35 C. Dogovski, S. C. Xie, G. Burgio, J. Bridgford, S. Mok, J. M. McCaw, K. Chotivanich, S. Kenny, N. Gnädig, J. Straimer, Z. Bozdech, D. A. Fidock, J. A. Simpson, A. M. Dondorp, S. Foote, N. Klonis and L. Tilley, *PLos Biol.*, 2015, **13**, e1002132.

36 A. Harikishore, M. Niang, S. Rajan, P. R. Preiser and H. S. Yoon, *Sci. Rep.*, 2013, **3**, 2501.

37 A. F. Cowman, D. Berry and J. Baum, *J. Cell Biol.*, 2012, **198**, 961–971.

38 J.-H. Liu, S.-T. Yang, H. Wang, Y. Chang, A. Cao and Y. Liu, *Nanomedicine*, 2012, **7**, 1801–1812.

39 F. Perreault, A. F. de Faria, S. Nejati and M. Elimelech, *ACS Nano*, 2015, **9**, 7226–7236.

40 F. Zhang, F. Liu, C. Wang, X. Xin, J. Liu, S. Guo and J. Zhang, *ACS Appl. Mater. Interfaces*, 2016, **8**, 2104–2110.

41 C. G. Salzmann, V. Nicolosi and M. L. H. Green, *J. Mater. Chem.*, 2010, **20**, 314–319.

42 L. H. Bannister, J. M. Hopkins, A. R. Dluzewski, G. Margos, I. T. Williams, M. J. Blackman, C. H. Kocken, A. W. Thomas and G. H. Mitchell, *J. Cell Sci.*, 2003, **116**, 3825–3834.

43 F. L. Schuster, *Clin. Microbiol. Rev.*, 2002, **15**, 355–364.

44 K. Singh, A. Agarwal, S. I. Khan, L. A. Walker and B. L. Tekwani, *J. Biomol. Screening*, 2007, **12**, 1109–1114.

45 S. A. Desai, *Sci. World J.*, 2013, **2013**, 363505.

46 P. T. Hammond, *Mater. Today*, 2012, **15**, 196–206.

47 Z. Ding, H. Ma and Y. Chen, *RSC Adv.*, 2014, **4**, 55290–55295.

48 R. Feng, Y. Yu, C. Shen, Y. Jiao and C. Zhou, *J. Biomed. Mater. Res., Part A*, 2015, **103**, 2006–2014.

49 M. Šimšíková, *Arch. Biochem. Biophys.*, 2016, **593**, 69–79.

50 A. El Tahir, P. Malhotra and V. Chauhan, *Malar. J.*, 2003, **2**, 11.

51 J. Liu, E. S. Istvan, I. Y. Gluzman, J. Gross and D. E. Goldberg, *Proc. Natl. Acad. Sci. U. S. A.*, 2006, **103**, 8840–8845.

52 S. E. Babbitt, L. Altenhofen, S. A. Cobbold, E. S. Istvan, C. Fennell, C. Doerig, M. Llinás and D. E. Goldberg, *Proc. Natl. Acad. Sci. U. S. A.*, 2012, **109**, E3278–E3287.

53 M. Rug, S. W. Prescott, K. M. Fernandez, B. M. Cooke and A. F. Cowman, *Blood*, 2006, **108**, 370–378.

54 Y. Zhang, C. Huang, S. Kim, M. Golkaram, M. W. A. Dixon, L. Tilley, J. Li, S. Zhang and S. Suresh, *Proc. Natl. Acad. Sci. U. S. A.*, 2015, **112**, 6068–6073.

55 A. Li, A. H. Mansoor, K. S. W. Tan and C. T. Lim, *J. Microbiol. Methods*, 2006, **66**, 434–439.